



Adsorption of Pb(II) From Aqueous Solutions Using Fe₃O₄@APTES@4-DMAB Nanomaterial

Celal Caner^{1,2} 

¹ Sakarya University, Faculty of Science, Department of Chemistry, Sakarya, Türkiye, ccaner@sakarya.edu.tr, ror.org/04ttnw109

² Sakarya University, Research, Development and Application Center (SARGEM), Sakarya, Türkiye, ror.org/04ttnw109

ARTICLE INFO

ABSTRACT

Keywords:

Heavy metal

Lead

Adsorption

Magnetic nanoparticles

4-Dimethylaminobenzaldehyde



Article History:

Received: 12.08.2025

Revised: 20.10.2025

Accepted: 26.11.2025

Online Available: 26.01.2026

This study investigates the synthesis and characterization of Fe₃O₄ nanoparticles coated with 3-aminopropyltriethoxysilane (APTES) and 4-dimethylaminobenzaldehyde (4-DMAB), aimed at their application in the adsorption of Pb(II) ions from aqueous solutions. The characterization of the Fe₃O₄@APTES@4-DMAB nanomaterial was conducted using several techniques, including field emission scanning electron microscopy (FESEM), energy dispersive X-ray spectroscopy (EDX), X-ray diffraction (XRD), and Fourier transform infrared spectroscopy (FT-IR). The synthesized spherical nanoparticles, measuring between 20 and 50 nm, exhibited stability without degradation during the coating process, and the successful coating with 4-DMAB was confirmed. Under optimal conditions—namely, a pH of 7, an adsorbent mass of 10 mg, and a contact duration of 30 minutes—the nanomaterial effectively adsorbed Pb(II) ions. The concentration of the metal ions was quantified using Inductively Coupled Plasma – Optical Emission Spectrometry (ICP-OES). To facilitate the recovery of the adsorbed Pb(II) ions, a desorption agent consisting of 0.5 mol/L HCl was utilized. Overall, the successfully synthesized and characterized Fe₃O₄@APTES@4-DMAB nanomaterial exhibited promising Pb(II) recovery results.

1. Introduction

In contemporary societies, industrialization and urbanization have led to a notable increase in pollutants entering the environment [1]. Among these pollutants, heavy metals present a significant threat to living organisms due to their widespread sources, high toxicity, persistence, inability to biodegrade, and propensity for bioaccumulation [2]. Heavy metals encompass a group of elements characterized by their high density. While certain metals such as zinc (Zn), copper (Cu), nickel (Ni), chromium (Cr), and cobalt (Co) are essential for biological functions, they can become toxic at elevated concentrations. In contrast, elements like arsenic (As), cadmium (Cd), lead (Pb), and mercury (Hg) are hazardous even at very low concentrations (parts per billion, ppb) [3]. When heavy metals accumulate in critical organs such as the liver, kidneys, and brain, they can result in severe health issues,

including growth retardation, nervous system damage, and cancer [4]. Thus, it is imperative to employ effective methods for removing heavy metals to mitigate their detrimental effects on environmental health and human well-being [5].

Lead is an extremely toxic heavy metal found in the earth's crust, and it has deadly effects on humans and other living organisms [6]. Humans have been exposed to the harmful effects of lead since they began processing the element over 5,000 years ago [7]. Lead ions can replace monovalent (Na⁺) and divalent (Ca²⁺, Fe²⁺, and Mg²⁺) cations in the body, inhibiting biological processes and disrupting the antioxidant system's balance by increasing the formation of free radicals [8]. Lead is used in various industrial applications, such as fuel additives, construction materials, ammunition, paint, and battery production. Humans can be exposed to lead by consuming contaminated food or water, inhaling

vehicle emissions, or directly contacting lead-containing materials [9]. According to the World Health Organization (WHO), the maximum permissible lead concentration in drinking water is 10 µg/L, while the threshold value for lead poisoning in blood is 10 µg/dL [2,10].

Among the commonly employed methods for heavy metal removal, several approaches are utilized, including chemical precipitation [11], membrane filtration [12], coagulation and flocculation [13], photocatalysis [14], electrochemical applications [15], ion exchange [16], and adsorption [17]. Each of these techniques has its distinct advantages and disadvantages [18]. Chemical precipitation can result in secondary pollution due to the precipitant, while slow ion removal rates often characterize ion exchange. Membrane filtration may lack stability, and electrochemical methods involve high energy consumption.

Flocculation and coagulation produce sludge, whereas photocatalytic methods require extended processing times. In contrast, adsorption stands out for its considerable benefits. It effectively removes heavy metal ions, even at low concentrations, and features straightforward processing requirements. The process is marked by rapid adsorption times, high capacity, and reusability through adsorption and desorption cycles. Furthermore, it demonstrates a strong affinity for the adsorbate, offers flexible design options, is cost-effective, and does not generate sludge [19]. Adsorption is fundamentally a reversible separation process whereby ions or molecules in a liquid or gas phase adhere to the surface of a solid material, referred to as the adsorbent. The reverse reaction, known as desorption, involves the release of the adhered ions or molecules, activating the surface for subsequent adsorption cycles [20].

Nanomaterials, defined as particles smaller than 100 nm, play a crucial role in enhancing the adsorption processes for heavy metal pollutants due to their distinctive sizes and physical properties [21]. Their effectiveness as adsorbents stems from a combination of factors: a high surface area-to-volume ratio, porosity, small size and shape, advanced structural characteristics, surface functionality, strong affinity for

pollutants, and reusability [22]. In particular, iron-based magnetic nanoparticles present a notable advantage, as they can be easily separated from solutions using an external magnetic field, thanks to their superparamagnetic behavior. This method offers a more convenient alternative to traditional separation techniques, such as filtration or centrifugation, which can be time-consuming [23]. Nonetheless, bare iron oxide nanoparticles are prone to agglomeration and oxidation due to their high surface energy and large surface area. To mitigate these challenges, functionalizing the surfaces of nanomaterials not only helps prevent agglomeration and oxidation but also enhances their selectivity for target heavy metal ions, thereby improving their overall adsorption capacity [24].

In this study, Fe₃O₄ nanoparticles were coated with 3-aminopropyltriethoxysilane (APTES) and 4-dimethylaminobenzaldehyde (4-DMAB), respectively, to synthesise a magnetic nanomaterial. This nanomaterial was characterised using field emission scanning electron microscopy (FESEM), energy dispersive X-ray spectroscopy (EDX), X-ray diffraction (XRD), and Fourier transform infrared spectroscopy (FT-IR) to obtain information about the size and morphology of the structure, chemical composition, crystal structure, and functional groups it contains. The successfully synthesised Fe₃O₄@APTES@4-DMAB was used as a nanoadsorbent to adsorb Pb(II) ions from aqueous solutions under optimal conditions.

2. Materials and Methods

2.1. Instrumentation

The morphology and size measurements of the magnetic nanoparticles synthesized in this study were performed using a Quanta FESEM (FEI, Japan). Elemental composition was analyzed with EDX (JEOL JSM 6060LV) connected to the FESEM system. The crystal structure was evaluated using a DMAX-2000 XRD (Rigaku D, Japan), while functional group analysis was conducted with a Spectrum 2 FT-IR spectrometer (Perkin Elmer, USA). Concentrations of Cd(II) and Pb(II) were determined using a Spectro

Arcos FHE-16 Inductively Coupled Plasma – Optical Emission Spectrometry (ICP-OES) (Spectro, Germany). pH values were measured with an Orion 2-Star pH meter (Thermo Fisher Scientific, USA). Ultra-pure water was produced using the Milli-Q® Advantage A10 water purification system (Merck, Germany). Solutions and suspensions were prepared with a Bandelin Sonorex Super RK 225 ultrasonic bath (Bandelin, Germany). A neodymium-iron-boron (Nd-Fe-B) magnet measuring 40 mm × 20 mm × 10 mm was utilized to separate nanoparticles. Furthermore, all glassware was meticulously cleaned by soaking it in a 3 mol/L nitric acid solution for 24 hours before use.

2.2. Materials and reagents

All chemicals employed in the experiments were of analytical purity and were procured from Merck (Germany). Iron (II) chloride tetrahydrate and iron (III) chloride hexahydrate were utilized as the iron sources for the synthesis of magnetite (Fe_3O_4). APTES and 4-DMAB were applied to coat the nanoparticles, and ethanol served as the solvent. Lead (II) solutions were prepared daily by diluting a 1000 mg/L stock solution. pH adjustments were achieved using 0.1 mol/L HCl and/or 0.1 mol/L NaOH.

2.3. Fe_3O_4 @APTES@4-DMAB synthesis

To synthesize Fe_3O_4 magnetic nanoparticles, 5.2 g of $\text{FeCl}_3 \cdot 6\text{H}_2\text{O}$ and 2 g of $\text{FeCl}_2 \cdot 4\text{H}_2\text{O}$ were dissolved in 25 mL of 0.4 mol/L HCl in an ultrasonic bath. Concurrently, 250 mL of 1.5 mol/L NaOH solution was prepared and stirred at 70 °C in an argon atmosphere. The iron solution was then added dropwise to the NaOH solution over 30 minutes to promote nanoparticle formation. Following the reaction, the iron nanoparticles were separated from the mixture using a magnet and washed with water until the pH was neutralized. Finally, the nanoparticles were dried at 60 °C for 24 hours, yielding 2.29 g [25].

In the second step, the objective was to coat the synthesized nanoparticles with APTES. 1.5 g of Fe_3O_4 was dispersed in 200 mL of a 1:1 ethanol-water mixture to accomplish this. Then, 0.6 g of APTES was added to the mixture, stirring at 70

°C for 24 hours. After this duration, the solid product was separated from the reaction medium through magnetic decantation. The solid was washed with ethanol and dried at 60 °C for 24 hours. Ultimately, 1.51 g of coated nanoparticles was obtained [26].

In the final step, 60 mL of a 5% solution of 4-DMAB was prepared in ethanol, adding 1 g of Fe_3O_4 @APTES. The mixture was stirred for 12 hours. The solid was separated from the reaction medium using a magnet, washed with ethanol three times, and dried at 60 °C for 24 hours. Ultimately, 0.92 g of the product was obtained [27].

The proposed mechanism of possible interaction of the Pb(II) ion with the nanomaterial is shown in Figure 1.

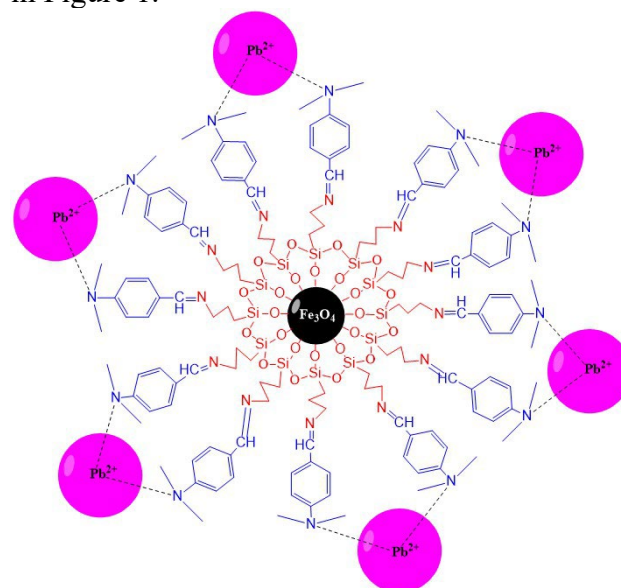


Figure 1. Fe_3O_4 @APTES@4-DMAB interaction with Pb(II)

2.4. Extraction procedure

A solution containing a final concentration of 1000 $\mu\text{g/L}$ of Pb(II) was adjusted to a pH of 7 using either 0.1 mol/L HCl or 0.1 mol/L NaOH, then diluted to a volume of 50 mL. 10 mg of Fe_3O_4 @APTES@4-DMAB were added to this solution. Magnetic solid-phase extraction was done by stirring the mixture at 200 rpm for 60 minutes to enhance the interaction between the metal ions and the adsorbent. The nanoparticles were separated from the solution using an external Nd magnet, and the resulting adsorption liquid was collected for analysis.

Subsequently, a desorption process was performed using 0.5 mol/L HCl for 30 minutes to recover the adsorbed analyte ions, allowing the Pb(II) ions retained by the adsorbent to return to the solution. The adsorption and desorption liquids were analyzed using an ICP-OES device [28].

Calculations for adsorption and desorption % recovery are conducted utilizing equations (1) and (2). In this context, c_0 represents the initial concentration of the adsorbate, c_e denotes the equilibrium concentration, and c_D signifies the concentration following the desorption process.

$$\%R = \frac{c_0 - c_e}{c_0} \times 100 \quad (1)$$

$$\%R = \frac{c_D}{c_0} \times 100 \quad (2)$$

3. Results and Discussion

3.1. Characterization

3.1.1. FESEM

The FESEM technique is employed to analyze the surfaces of a diverse range of samples by investigating the morphology and structure of materials. This advanced imaging method facilitates the acquisition of high-resolution images [29]. In this study, FESEM images were captured for each of the synthesized Fe_3O_4 , $\text{Fe}_3\text{O}_4@$ APTES, and $\text{Fe}_3\text{O}_4@$ APTES@4-DMAB nanoparticles, yielding valuable insights into the materials and their coating conditions (Figure 2). The uncoated Fe_3O_4 nanoparticles typically exhibit a spherical shape, while those produced via a standard precipitation method display defined, sharp edges. These synthesized nanoparticles range in size from approximately 20 to 50 nm, with some showing a propensity to aggregate. In the FESEM image of $\text{Fe}_3\text{O}_4@$ APTES, the particles exhibit more pronounced, slightly irregular, and blurred edges, suggesting that the APTES coating has formed a layer on the surface of the particles.

Although the overall shape remains predominantly spherical or nearly so, the APTES coating introduces a slightly rough or amorphous structure, indicating surface functionalization.

For the $\text{Fe}_3\text{O}_4@$ APTES@4-DMAB nanoparticles, the FESEM image reveals that while the particles still appear spherical, their edges have become thicker and less defined than in previous images. This phenomenon is attributed to the increased electron density resulting from the C=N bond formed on the surface and the binding of 4-DMAB molecules to the nanoparticles. The functionalization process has enhanced the surface area and the abundance of functional groups, leading to greater interaction areas for target analytes.

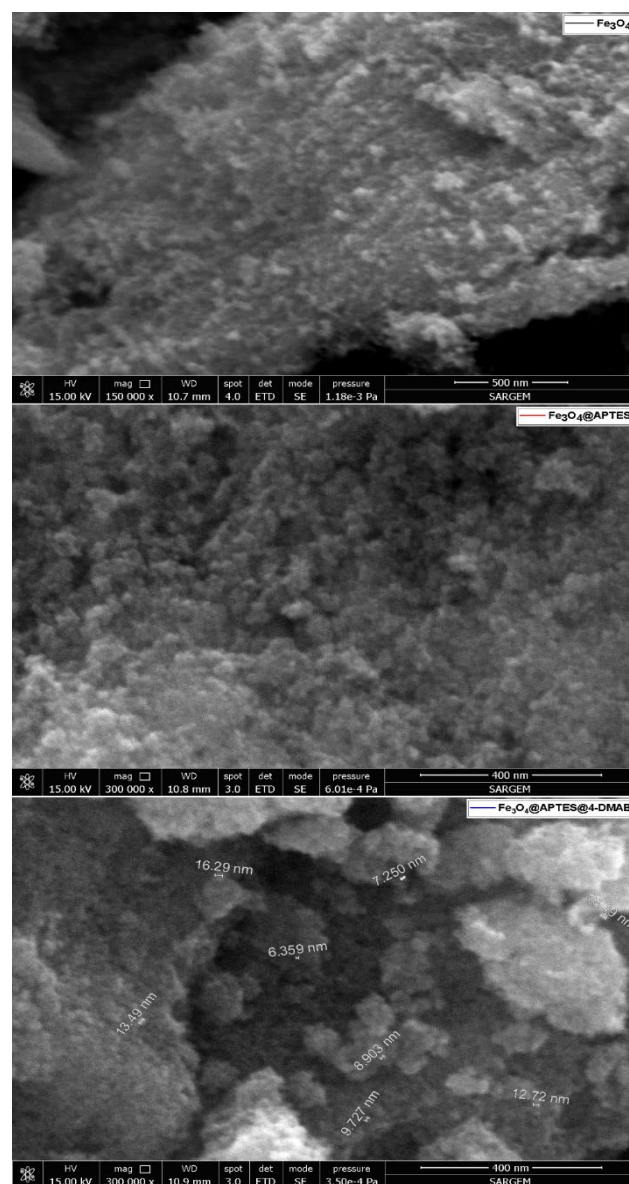


Figure 2. FESEM images of Fe_3O_4 , $\text{Fe}_3\text{O}_4@$ APTES and $\text{Fe}_3\text{O}_4@$ APTES@4-DMAB nanoparticles

3.1.2. EDX

The EDX technique effectively reveals materials' composition and elemental distribution through an X-ray detector [30]. All EDX spectra are

shown in Figure 3. The EDX spectrum of Fe₃O₄ nanoparticles indicates that they are composed exclusively of iron and oxygen atoms, with a composition of 78.68% iron and 21.32% oxygen by weight. These results are closely aligned with the theoretical values for Fe₃O₄, which are 72.36% iron and 27.64% oxygen by weight. In the spectrum for Fe₃O₄@APTES, peaks for silicon (Si) and nitrogen (N) confirm that the magnetic nanoparticles have been successfully coated with APTES. The Fe₃O₄@APTES nanoparticles comprise 71.30% iron, 24.61% oxygen, 2.84% nitrogen, and 1.25% silicon by weight. Furthermore, the spectrum for Fe₃O₄@APTES@4-DMAB indicates that the synthesized nanoparticles contain 68.34% iron, 25.97% oxygen, 1.76% silicon, and 3.93% nitrogen by weight. The increase in the nitrogen percentage in this spectrum relative to the previous one suggests that the coating with 4-DMAB has been accomplished.

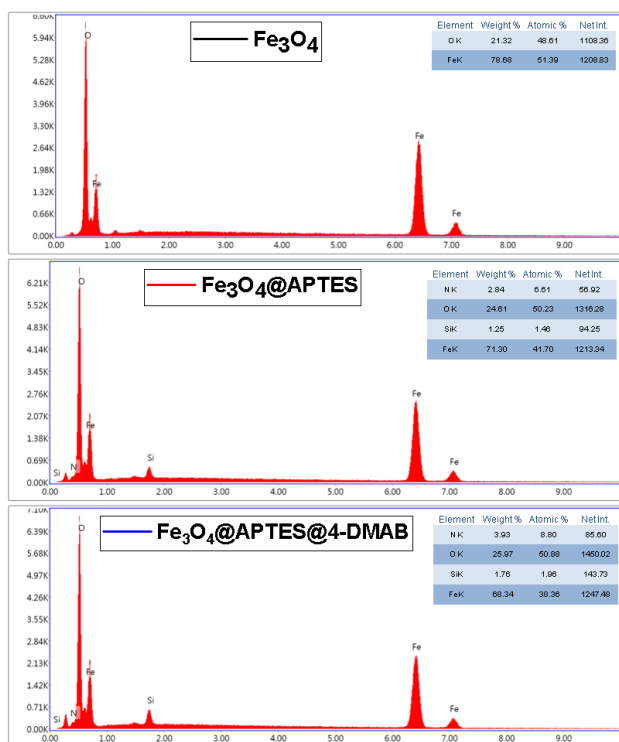


Figure 3. EDX spectra of Fe₃O₄, Fe₃O₄@APTES and Fe₃O₄@APTES@4-DMAB nanoparticles

3.1.3. XRD

XRD offers crucial insights into the particle size and distribution and the shape and structure of materials, enhanced by small-angle neutron scattering [31]. The XRD spectrum for each nanoparticle synthesized in this study is

presented in Figure 4. Peaks detected at 2θ angles of 18.29°, 30.39°, 35.78°, 43.29°, 53.81°, 57.51°, 62.93°, and 75.67° correspond to the (111), (220), (311), (400), (511), (440), and (622) lattice planes, respectively. This data confirms that every synthesized material exhibits the spinel face-centered cubic structure characteristic of Fe₃O₄. These nanoparticles have a JCPDS card number 01-075-0449. The findings indicate that the synthesis of Fe₃O₄ nanoparticles was successful, and no degradation occurred following the coating process. Furthermore, applying the Scherrer equation (3), the particle size was determined to be 10.61 nm, while the lattice constant of the crystal structure was established at 0.25 nm.

In the Scherrer equation, B represents the full width at half maximum (FWHM), k is the Scherrer constant, D denotes the crystallite size, and T corresponds to the wavelength of the X-ray used.

$$D = \frac{k\lambda}{B \cos \theta} \quad (3)$$

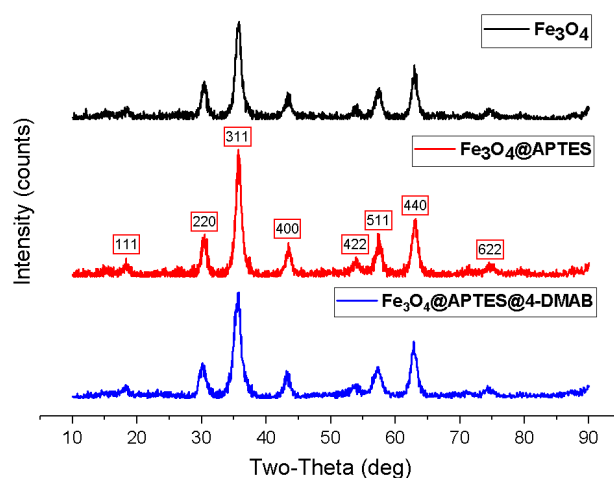


Figure 4. XRD spectra of Fe₃O₄, Fe₃O₄@APTES and Fe₃O₄@APTES@4-DMAB nanoparticles

3.1.4. FT-IR

FT-IR spectroscopy is extensively utilized for material characterization due to its versatility and high efficiency. When an infrared (IR) beam is directed at a sample, absorption occurs in the sample's functional groups, resulting in stretching, bending, deformation, or vibration modes at wave numbers from 4000 to 400 cm⁻¹. This capability allows for the straightforward detection of molecules bound to nanoparticles

[32]. Figure 5 illustrates the FT-IR spectra for Fe_3O_4 , $\text{Fe}_3\text{O}_4@\text{APTES}$, 4-DMAB, and $\text{Fe}_3\text{O}_4@\text{APTES}@4\text{-DMAB}$. The bands observed at 550 and 625 cm^{-1} in the Fe_3O_4 spectrum are associated with Fe-O stretching vibrations, while the band at 3412 cm^{-1} corresponds to O-H stretching vibrations. In the $\text{Fe}_3\text{O}_4@\text{APTES}$ spectrum, the band at 1001 cm^{-1} indicates Si-O stretching vibrations, and the bands at 2924 and 2880 cm^{-1} are attributed to C-H stretching vibrations, confirming the successful coating of Fe_3O_4 nanoparticles with APTES. The spectrum for 4-DMAB reveals characteristic bands at 2905, 2797, and 2712 cm^{-1} related to aromatic and aliphatic C-H stretching. The band at 1658 cm^{-1} corresponds to C=O stretching, while the bands at 1588 and 1528 cm^{-1} are associated with C=C stretching. Additionally, the band at 1362 cm^{-1} pertains to C-H bending, the band at 1230 cm^{-1} corresponds to C-N stretching, and the band at 810 cm^{-1} relates to aromatic C-H bending vibrations. In the $\text{Fe}_3\text{O}_4@\text{APTES}@4\text{-DMAB}$ spectrum, all stretching vibrations from Fe-O in Fe_3O_4 , Si-O in APTES, and C=C in 4-DMAB are present. The distinct band at 1605 cm^{-1} corresponds to C=N stretching vibrations, which confirms the successful completion of the reaction.

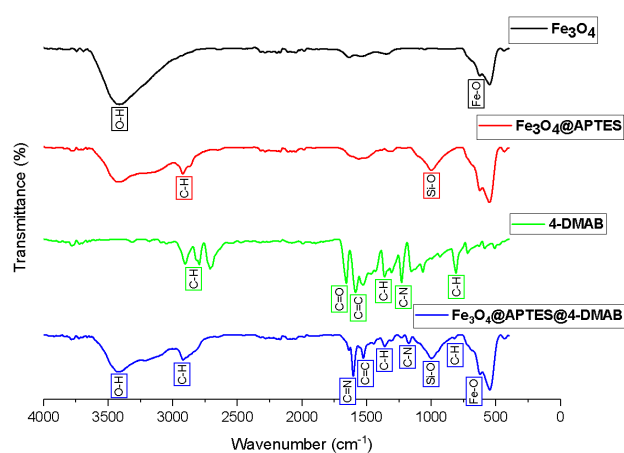


Figure 5. FT-IR spectra of Fe_3O_4 , $\text{Fe}_3\text{O}_4@\text{APTES}$ and $\text{Fe}_3\text{O}_4@\text{APTES}@4\text{-DMAB}$ nanoparticles

3.2. Optimization

3.2.1. pH

The adsorption of heavy metals by an adsorbent is significantly influenced by the pH of the surrounding environment, making it crucial to examine the effect of pH on metal ion removal [33]. At low pH levels, the functional groups on

the nanoparticle surfaces are primarily protonated; this leads to a lack of electrostatic repulsion forces between the adsorbent and the metal ions that could hinder adsorption. Furthermore, competition for adsorption can arise between the target metal ions and hydronium ions (H_3O^+). In contrast, complex structures may form at elevated pH levels between metal species and hydroxide (OH^-) groups, which can block the active sites on the adsorbent and diminish its adsorption capacity. The study assessed pH values ranging from 2 to 10, with the highest recovery rate observed at pH 7 (Figure 6). This suggests that Pb(II) ions effectively interact with the adsorbent at neutral pH, allowing for their removal from the solution. Additionally, in a separate study, Saberi-Zare et al grafted cyanoguanidine (CG) and salicylaldehyde (SA) Schiff bases onto chitosan magnetic nanocomposites, resulting in the formation of a hybrid magnetic nanostructure [34]. They employed this synthesized nanostructure to remove Pb(II) and Cd(II) ions, reporting that it adsorbed the analyte ions at pH 7. However, a decline in recovery at higher pH levels was attributed to the precipitation of metal ions as hydroxides.

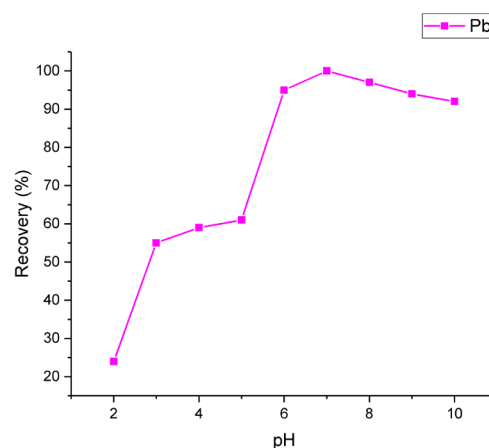


Figure 6. The effect of pH on the adsorption of Pb(II) ions. (adsorbent amount: 10 mg, contact time: 30 min, Pb(II) concentration: 1000 $\mu\text{g/L}$)

3.2.2. Adsorbent amount

Adsorbents are materials that capture target analytes on their surfaces due to the presence of active sites and functional groups, effectively isolating these analytes from their surrounding environment. Recent studies focused on optimizing the minimum amount of adsorbent

necessary to achieve the highest recovery of target heavy metal ions. Utilizing insufficient amounts of adsorbent results in a limited number of active sites, while excessive quantities can cause nanoparticle aggregation, leading to a reduction in total surface area and, consequently, lower recovery rates [35]. In this study, the amount of $\text{Fe}_3\text{O}_4@\text{APTES}@4\text{-DMAB}$ magnetic nanoparticles was varied at 1, 3, 5, 10, 20, and 30 mg to identify the optimal adsorbent quantity (Figure 7). It was determined that 100% recovery of Pb(II) ions was achieved with 10 mg and above, prompting using 10 mg for subsequent experiments. Additionally, a study conducted by Jiang et al involved the synthesis of the magnetic metal-organic framework $\text{Fe}_3\text{O}_4@\text{ZIF-8}$ to examine the removal of Pb(II) and Cu(II) ions from wastewater, also using 10 mg of this material as the optimized adsorbent amount [36].

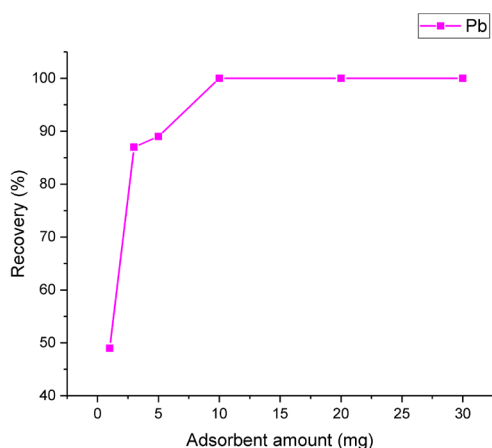


Figure 7. The effect of adsorbent amount on the adsorption of Pb(II) ions. (pH: 7, contact time: 30 min, Pb(II) concentration: 1000 $\mu\text{g/L}$)

3.2.3. Contact time

The contact time between heavy metal ions and the adsorbent plays a crucial role in adsorption. As the contact time increases, the duration of interaction between analyte ions and the active sites on the nanoadsorbent also extends, resulting in higher recovery rates. The swift recovery observed in the initial stages is due to the abundance of accessible vacant sites on the adsorbent surface at that point. However, the adsorption rate tends to diminish over time [37]. In this study, the adsorption of Pb(II) ions onto the active sites of $\text{Fe}_3\text{O}_4@\text{APTES}@4\text{-DMAB}$ was assessed at contact times of 5, 10, 15, 20, 30, 45, and 60 minutes (Figure 8). The adsorption

process peaked at 30 minutes and remained constant thereafter, establishing this duration as the optimal contact time for subsequent experiments. Likewise, in a related study, Hosseini and colleagues synthesized a novel $\text{Fe}_3\text{O}_4@\text{starch}@eggshell$ magnetic nanocomposite, which demonstrated effectiveness as an adsorbent for the removal of Cd(II) and Pb(II) heavy metal ions. They found that a contact time of 60 minutes was optimal for their investigations [38].

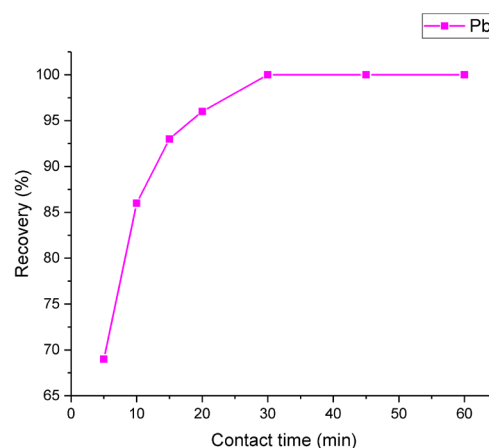


Figure 8. The effect of contact time on the adsorption of Pb(II) ions. (pH: 7, adsorbent amount: 10 mg, Pb(II) concentration: 1000 $\mu\text{g/L}$)

3.2.4. Desorption

Selecting the most suitable eluent for the desorption of heavy metal ions that an adsorbent has selectively retained is essential. This selection depends on the type of adsorbent used, the specific analyte involved, and the underlying adsorption mechanism. During adsorption, the adsorbent and target metal ions can interact in various ways, including bond reactions, electrostatic interactions, and hydrogen bonds. It is essential to utilize appropriate desorption agents—such as alkalis, acids, organic solvents, and complexing agents—that are cost-effective and gentle on the adsorbent structure, while exhibiting a high affinity for the analyte [39]. The study used HCl and NaOH at varying concentrations as acidic and basic desorption agents, respectively. The results presented in Table 1 show that the acidic agent outperformed the basic agent in desorbing Pb(II) ions, with the highest recovery achieved at a concentration of 0.5 mol/L. The superior effectiveness of the acidic desorption agent can be attributed to the

increased concentration of hydronium ions, which compete with Pb(II) ions for desorption from the adsorbent surface. Additionally, Shi et al developed a novel amino-functionalized $\text{Fe}_3\text{O}_4@\text{MnO}_2@\text{SiO}_2@\text{NH}_2$ adsorbent to recover Pb(II), Cu(II), and Ni(II) ions, using 1 mol/L nitric acid for the desorption of these bound metal ions during the desorption process [40].

Table 1. Recoveries of Pb(II) at different concentrations of desorption agents. (pH: 7, adsorbent amount: 10 mg, contact time: 30 min, Pb(II) concentration of 1000 $\mu\text{g/L}$).

Concentration (mol/L)	% Recovery	
	HCl	NaOH
0.1	84	1
0.25	97	2
0.5	100	2
1	90	2
2	90	3

4. Conclusion

$\text{Fe}_3\text{O}_4@\text{APTES}@4\text{-DMAB}$ nanoparticles were synthesized to effectively recover Pb(II) ions, which are recognized as heavy metals and can adversely affect both the environment and living organisms, even at minimal concentrations in aqueous solutions. The synthesized nanoparticles were characterized using FESEM, EDX, XRD, and FT-IR. The analysis revealed that the spherical nanoparticles, measuring 20 to 50 nm in diameter, were functionalized with the 4-DMAB ligand, facilitating interaction with the target Pb(II) ions. The $\text{Fe}_3\text{O}_4@\text{APTES}@4\text{-DMAB}$ nanomaterial was utilized to adsorb Pb(II) ions from aqueous solutions under optimal conditions of pH 7, an adsorbent amount of 10 mg, and a contact time of 30 minutes. Desorption of the adsorbed Pb(II) ions was successfully carried out using 5 mL of 0.5 M hydrochloric acid. The findings suggest that the synthesized nanomaterial is an effective adsorbent for recovering Pb(II) ions.

Article Information Form

Acknowledgments

The author would like to thank Gamze Naycı for her contributions.

The Declaration of Conflict of Interest/ Common Interest

No conflict of interest or common interest has been declared by the author.

Artificial Intelligence Statement

No artificial intelligence tools were used while writing this article.

Copyright Statement

The author owns the copyright of their work published in the journal and their work is published under the CC BY-NC 4.0 license.

References

- [1] X. Shen, et al., "A critical review on the phytoremediation of heavy metals from environment: Performance and challenges," *Chemosphere*, vol. 291, no. 3, p. 132979, Mar 2022. doi: 10.1016/j.chemosphere.2021.132979. [Online]. Available: <https://doi.org/10.1016/j.chemosphere.2021.132979>
- [2] X. Feng, R. Long, L. Wang, C. Liu, Z. Bai, and X. Liu, "A review on heavy metal ions adsorption from water by layered double hydroxide and its composites," *Sep. Purif. Technol.*, vol. 284, p. 120099, Feb 2022. doi: 10.1016/j.seppur.2021.120099. [Online]. Available: <https://doi.org/10.1016/j.seppur.2021.120099>
- [3] F.-J. Zhao, Z. Tang, J.-J. Song, X.-Y. Huang, and P. Wang, "Toxic metals and metalloids: Uptake, transport, detoxification, phytoremediation, and crop improvement for safer food," *Mol. Plant.*, vol. 15, no. 1, pp. 325-344, Jan 2022. doi: 10.1016/j.molp.2021.09.016. [Online]. Available: <https://doi.org/10.1016/j.molp.2021.09.016>
- [4] S. Bala, et al., "Recent strategies for bioremediation of emerging pollutants: A review for a green and sustainable environment," *Toxics*, vol. 10, no. 8, p. 484, Aug 2022. doi:

- 10.3390/toxics10080484. [Online]. Available: <https://doi.org/10.3390/toxics10080484>
- [5] K. Aziz, F. Mustafa, K. M. Omer, S. Hama, R. F. Hamarawf, and K. O. Rahman, "Heavy metal pollution in the aquatic environment: Efficient and low-cost removal approaches to eliminate their toxicity: A review," *RSC Adv.*, vol. 13, no. 26, pp. 17595–17610, June 2023. doi: 10.1039/D3RA00723E. [Online]. Available: <https://doi.org/10.1039/d3ra00723e>.
- [6] N. S. N. Yusoff, V. F. Knight, S. Mohamed, and W. Md, "Heavy metal toxicity and its treatment," *Adv. Hum. Biol.*, vol. 14, no. 4, pp. 295–301, Nov. 2024. doi: 10.4103/aihb.aihb_70_24. [Online]. Available: https://doi.org/10.4103/aihb.aihb_70_24
- [7] M. S. Collin, et al., "Bioaccumulation of lead (Pb) and its effects on human: A review," *J. Hazard. Mater. Adv.*, vol. 7, p. 100094, Aug 2022. doi: 10.1016/j.hazadv.2022.100094. [Online]. Available: <https://doi.org/10.1016/j.hazadv.2022.100094>
- [8] L. Iddrisu, F. Danso, K.-L. Cheong, Z. Fang, and S. Zhong, "Polysaccharides as protective agents against heavy metal toxicity," *Foods*, vol. 13, no. 6, p. 853, Mar 2024. doi: 10.3390/foods13060853. [Online]. Available: <https://doi.org/10.3390/foods13060853>
- [9] K. Renu, et al., "Molecular mechanism of heavy metals (Lead, Chromium, Arsenic, Mercury, Nickel and Cadmium) - induced hepatotoxicity – A review," *Chemosphere*, vol. 271, p. 129735, May 2021. doi: 10.1016/j.chemosphere.2021.129735. [Online]. Available: <https://doi.org/10.1016/j.chemosphere.2021.129735>
- [10] M. Balali-Mood, K. Naseri, Z. Tahergorabi, M. R. Khazdair, and M. Sadeghi, "Toxic mechanisms of five heavy metals: Mercury, Lead, Chromium, Cadmium, and Arsenic," *Front. Pharmacol.*, vol. 12, p. 643972, Apr 2021. doi: 10.3389/fphar.2021.643972. [Online]. Available: <https://doi.org/10.3389/fphar.2021.643972>
- [11] A. Pohl, "Removal of heavy metal ions from water and wastewaters by sulfur-containing precipitation agents," *Water Air Soil Pollut.*, vol. 231, no. 10, p. 497, Oct 2020. doi: 10.1007/s11270-020-04863-w. [Online]. Available: <https://doi.org/10.1007/s11270-020-04863-w>
- [12] S. Hong, F. Al Marzooqi, J. K. El-Demellawi, N. Al Marzooqi, H. A. Arafat, and H. N. Alshareef, "Ion-selective separation using MXene-based membranes: A review," *ACS Mater. Lett.*, vol. 5, no. 2, pp. 341–356, 2023. doi: 10.1021/acsmaterialslett.2c00914. [Online]. Available: <https://doi.org/10.1021/acsmaterialslett.2c00914>
- [13] R. Shrestha, et al., "Technological trends in heavy metals removal from industrial wastewater: A review," *J. Environ. Chem. Eng.*, vol. 9, no. 4, p. 105688, Aug 2021. doi: 10.1016/j.jece.2021.105688. [Online]. Available: <https://doi.org/10.1016/j.jece.2021.105688>
- [14] A. Azimi, A. Azari, M. Rezakazemi, and M. Ansarpour, "Removal of heavy metals from industrial wastewaters: A review," *ChemBioEng Rev.*, vol. 4, no. 1, pp. 37–59, 2017. doi: 10.1002/cben.201600010. [Online]. Available: <https://doi.org/10.1002/cben.201600010>
- [15] J. S. D. Jeremias, J.-Y. Lin, M. L. P. Dalida, and M.-C. Lu, "Abatement technologies for copper containing industrial wastewater effluents – A review," *J. Environ. Chem. Eng.*, vol. 11, no. 2, p. 109336, Apr 2023. doi:

- 10.1016/j.jece.2023.109336. [Online]. Available: <https://doi.org/10.1016/j.jece.2023.109336>
- [16] A. Bashir, et al., "Removal of heavy metal ions from aqueous system by ion-exchange and biosorption methods," *Environ. Chem. Lett.*, vol. 17, no. 2, pp. 729–754, June 2019. doi: 10.1007/s10311-018-00828-y. [Online]. Available: <https://doi.org/10.1007/s10311-018-00828-y>
- [17] D. Fan, Y. Peng, X. He, J. Ouyang, L. Fu, and H. Yang, "Recent progress on the adsorption of heavy metal ions Pb(II) and Cu(II) from wastewater," *Nanomaterials*, vol. 14, no. 12, p. 1037, 2024. doi: 10.3390/nano14121037. [Online]. Available: <https://doi.org/10.3390/nano14121037>
- [18] S. S. Fiyadh, et al., "Review on heavy metal adsorption processes by carbon nanotubes," *J. Clean. Prod.*, vol. 230, pp. 783–793, Sept 2019. doi: 10.1016/j.jclepro.2019.05.154. [Online]. Available: <https://doi.org/10.1016/j.jclepro.2019.05.154>
- [19] L. Velarde, M. S. Nabavi, E. Escalera, M.-L. Antti, and F. Akhtar, "Adsorption of heavy metals on natural zeolites: A review," *Chemosphere*, vol. 328, p. 138508, July 2023. doi: 10.1016/j.chemosphere.2023.138508. [Online]. Available: <https://doi.org/10.1016/j.chemosphere.2023.138508>
- [20] M. Z. A. Zaimee, M. S. Sarjadi, and M. L. Rahman, "Heavy metals removal from water by efficient adsorbents," *Water*, vol. 13, no. 19, p. 2659, Sept 2021. doi: 10.3390/w13192659. [Online]. Available: <https://doi.org/10.3390/w13192659>
- [21] J. Sadiq, A. F. Qader, R. A. Omer, and A. Ali, "Magnetic nanoparticles for efficient heavy metal removal: Synthesis, adsorption capacity, and key experimental parameters," *Rev. Inorg. Chem.*, 2024. doi: 10.1515/revic-2024-0090. [Online]. Available: <https://doi.org/10.1515/revic-2024-0090>
- [22] M. B. Mensah, D. J. Lewis, N. O. Boadi, and J. A. M. Awudza, "Heavy metal pollution and the role of inorganic nanomaterials in environmental remediation," *R. Soc. Open Sci.*, vol. 8, no. 10, p. 201485, Oct 2021. doi: 10.1098/rsos.201485. [Online]. Available: <https://doi.org/10.1098/rsos.201485>
- [23] J. Nikić, M. Watson, A. Tubić, M. Šolić, and J. Agbaba, "Recent trends in the application of magnetic nanocomposites for heavy metals removal from water: A review," *Sep. Sci. Technol.*, vol. 59, no. 2, pp. 1–39, Mar 2024. doi: 10.1080/01496395.2024.2315626. [Online]. Available: <https://doi.org/10.1080/01496395.2024.2315626>
- [24] T. B. Mbuyazi and P. A. Ajibade, "Magnetic iron oxides nanocomposites: Synthetic techniques and environmental applications for wastewater treatment," *Discover Nano*, vol. 19, no. 1, p. 153, Sept 2024. doi: 10.1186/s11671-024-04102-9. [Online]. Available: <https://doi.org/10.1186/s11671-024-04102-9>
- [25] C. Caner, M. S. Dundar, H. Altundag, and M. Soylak, "Determination of Arsenic in milk by magnetic solid-phase extraction (MSPE) with novel iron (II, III) nanoparticles coated with tween 80," *Anal. Lett.*, vol. 58, no. 6, pp. 1077–1091, May 2024. doi: 10.1080/00032719.2024.2351106. [Online]. Available: <https://doi.org/10.1080/00032719.2024.2351106>
- [26] Y. Liu, Y. Li, X.-M. Li, and T. He, "Kinetics of (3-Aminopropyl) triethoxysilane (APTES) silanization of superparamagnetic iron oxide nanoparticles," *Langmuir*, vol. 29, no. 49,

- pp. 15275–15282, Nov 2013. doi: 10.1021/la403269u. [Online]. Available: <https://doi.org/10.1021/la403269u>
- [27] M. Ozmen, K. Can, G. Arslan, A. Tor, Y. Cengeloglu, and M. Ersoz, "Adsorption of Cu(II) from aqueous solution by using modified Fe₃O₄ magnetic nanoparticles," *Desalination*, vol. 254, nos. 1–3, pp. 162–169, 2010. [Online]. Available: <https://doi.org/10.1016/j.desal.2009.11.043>
- [28] C. S. Keskin, "Rapid removal of Cd²⁺, Pb²⁺ and Cr³⁺ by polymer/Fe₃O₄ composite," *J. Water Chem. Technol.*, vol. 41, no. 5, pp. 299–306, Sept 2019. doi: 10.3103/s1063455x19050059. [Online]. Available: <https://doi.org/10.3103/s1063455x19050059>
- [29] M. Nikshitha, S. M. Sudhakara, and M. S. Shetty, "Organic-inorganic hybrids: A comprehensive review on synthesis and their potential applications," *Mater. Chem. Phys.*, vol. 331, p. 130181, Feb 2025. doi: 10.1016/j.matchemphys.2024.130181. [Online]. Available: <https://doi.org/10.1016/j.matchemphys.2024.130181>
- [30] M. Iwanow, T. Gärtner, V. Sieber, and B. König, "Activated carbon as catalyst support: precursors, preparation, modification and characterization," *Beilstein J. Org. Chem.*, vol. 16, pp. 1188–1202, June 2020. doi: 10.3762/bjoc.16.104. [Online]. Available: <https://doi.org/10.3762/bjoc.16.104>
- [31] P. R. S. Baabu, H. K. Kumar, M. B. Gumpu, K. J. Babu, A. J. Kulandaisamy, and J. B. B. Rayappan, "Iron oxide nanoparticles: A review on the province of its compounds, properties and biological applications," *Materials*, vol. 16, no. 1, p. 59, 2023. doi: 10.3390/ma16010059. [Online]. Available: <https://doi.org/10.3390/ma16010059>
- [32] N. K. Sharma, J. Vishwakarma, S. Rai, T. S. Alomar, N. AlMasoud, and A. Bhattarai, "Green route synthesis and characterization techniques of silver nanoparticles and their biological adeptness," *ACS Omega*, vol. 7, no. 31, pp. 27004–27020, 2022. doi: 10.1021/acsomega.2c01400. [Online]. Available: <https://doi.org/10.1021/acsomega.2c01400>
- [33] M. A. Tahooun, S. M. Siddeeg, N. S. Alsaiani, W. Mnif, and F. B. Rebah, "Effective heavy metals removal from water using nanomaterials: A Review," *Processes*, vol. 8, no. 6, p. 645, May 2020. doi: 10.3390/pr8060645. [Online]. Available: <https://doi.org/10.3390/pr8060645>
- [34] M. Saberi-Zare and M. A. Bodaghifard, "A Schiff base-functionalized chitosan magnetic bio-nanocomposite for efficient removal of Pb (II) and Cd (II) ions from aqueous solutions," *Int. J. Biol. Macromol.*, p. 139794, Jan. 2025. doi: 10.1016/j.ijbiomac.2025.139794. [Online]. Available: <https://doi.org/10.1016/j.ijbiomac.2025.139794>
- [35] M. M. Youssif, H. G. El-Attar, V. Hessel, and M. Wojnicki, "Recent developments in the adsorption of heavy metal ions from aqueous solutions using various nanomaterials," *Materials*, vol. 17, no. 21, p. 5141, Oct. 2024. doi: 10.3390/ma17215141. [Online]. Available: <https://doi.org/10.3390/ma17215141>
- [36] X. Jiang et al., "Magnetic metal-organic framework (Fe₃O₄@ZIF-8) core-shell composite for the efficient removal of Pb(II) and Cu(II) from water," *J. Environ. Chem. Eng.*, vol. 9, no. 5, p. 105959, Oct. 2021. doi: 10.1016/j.jece.2021.105959. [Online]. Available: <https://doi.org/10.1016/j.jece.2021.105959>

- [37] S. Wadhawan, A. Jain, J. Nayyar, and S. K. Mehta, "Role of nanomaterials as adsorbents in heavy metal ion removal from waste water: A review," *J. Water Process Eng.*, vol. 33, p. 101038, Feb 2020. doi: 10.1016/j.jwpe.2019.101038. [Online]. Available: <https://doi.org/10.1016/j.jwpe.2019.101038>
- [38] S. S. Hosseini, A. Hamadi, R. Foroutan, Seyed Jamaledin Peighambardoust, and Bahman Ramavandi, "Decontamination of Cd²⁺ and Pb²⁺ from aqueous solution using a magnetic nanocomposite of eggshell/starch/Fe₃O₄," *J. Water Process Eng.*, vol. 48, p. 102911, June 2022. doi: 10.1016/j.jwpe.2022.102911. [Online]. Available: <https://doi.org/10.1016/j.jwpe.2022.102911>
- [39] S. Yadav, N. Sharma, A. Dalal, P. Panghal, A. K. Sharma, and S. Kumar, "Cutting-edge regeneration technologies for saturated adsorbents: A systematic review on pathways to circular wastewater treatment system," *Environ. Monit. Assess.*, vol. 197, p. 215, 2025. [Online]. Available: <https://doi.org/10.1007/s10661-025-13657-8>
- [40] H. Shi et al., "The preparation of Fe₃O₄-MnO₂-SiO₂-NH₂ for selective adsorption of Pb(II) in mixed solution of Pb(II), Cu(II), and Ni(II)," *Water Air Soil Pollut.*, vol. 234, no. 6, p. 385, June 2023. doi: 10.1007/s11270-023-06353-1. [Online]. Available: <https://doi.org/10.1007/s11270-023-06353-1>